Extending the long-term record of volcanic SO$_2$ emissions with the Ozone Mapping and Profiler Suite nadir mapper

S. A. Carn[1,2], K. Yang[3], A. J. Prata[4], and N. A. Krotkov[5]

[1]Department of Geological and Mining Engineering and Sciences, Michigan Technological University, Houghton, Michigan, USA, [2]Department of Mineral Sciences, National Museum of Natural History, Smithsonian Institution, Washington, District of Columbia, USA, [3]Department of Atmospheric and Oceanic Science, University of Maryland College Park, College Park, Maryland, USA, [4]Atmosphere and Climate Department, Norwegian Institute for Air Research, Kjeller, Norway, [5]Armospheric Chemistry and Dynamics Laboratory, Code 614, NASA Goddard Space Flight Center, Greenbelt, Maryland, USA

Abstract Uninterrupted, global space-based monitoring of volcanic sulfur dioxide (SO$_2$) emissions is critical for climate modeling and aviation hazard mitigation. We report the first volcanic SO$_2$ measurements using ultraviolet (UV) Ozone Mapping and Profiler Suite (OMPS) nadir mapper data. OMPS was launched on the Suomi National Polar-orbiting Partnership satellite in October 2011. We demonstrate the sensitivity of OMPS SO$_2$ measurements by quantifying SO$_2$ emissions from the modest eruption of Paluweh volcano (Indonesia) in February 2013 and tracking the dispersion of the volcanic SO$_2$ cloud. The OMPS SO$_2$ retrievals are validated using Ozone Monitoring Instrument and Atmospheric Infrared Sounder measurements. The results confirm the ability of OMPS to extend the long-term record of volcanic SO$_2$ emissions based on UV satellite observations. We also show that the Paluweh volcanic SO$_2$ reached the lower stratosphere, further demonstrating the impact of small tropical volcanic eruptions on stratospheric aerosol optical depth and climate.

1. Introduction

Maintaining continuous, global satellite-based monitoring of volcanic sulfur dioxide (VSO$_2$) emissions is critical for climate modeling and aviation hazard mitigation. Periodic injections of SO$_2$ into the stratosphere by explosive volcanic eruptions are the major driver of modulations in stratospheric aerosol optical depth (SAOD), which impacts climate through direct radiative forcing [e.g., *Robock*, 2000]. Volcanic eruption clouds are also hazards to aviation, and timely monitoring of their location and composition using satellite remote sensing is crucial for aircraft safety.

Here we present the first retrievals of VSO$_2$ using data from the Ozone Mapping and Profiler Suite (OMPS) nadir mapper (NM), an ultraviolet (UV) sensor aboard the Suomi National Polar-orbiting Partnership (SNPP) spacecraft. We show that the OMPS-NM SO$_2$ measurements are suitable for extension of the comprehensive inventory of volcanic SO$_2$ emissions based on UV satellite measurements made since 1978 (Figure 1) [*Bluth et al.*, 1993; *Carn et al.*, 2003]. While several spaceborne infrared (IR) sensors, including the Atmospheric Infrared Sounder (AIRS on Aqua) and Infrared Atmospheric Sounding Interferometer (on MetOp-A/B), can also measure VSO$_2$ very effectively [e.g., *Prata and Bernardo*, 2007; *Clarisse et al.*, 2012], maintaining a UV measurement capability for volcanic SO$_2$ is essential since UV and IR techniques have complementary sensitivity and coverage. Specifically, UV sensors have lower detection limits and higher sensitivity to lower tropospheric SO$_2$ than IR retrievals, permitting detection of small eruptions, and are typically more effective at tracking volcanic clouds in cloudy and/or moist atmospheres (e.g., in the tropics). Furthermore, current spaceborne UV SO$_2$ measurements are also compromised. Although the Ozone Monitoring Instrument (OMI on NASA's Aura satellite) continues to collect data at the time of writing, since 2008, its spatial coverage has been reduced by the "row anomaly" (a partial blockage in the sensor's field of view (FOV) (see http://www.knmi.nl/omi/research/product/rowanomaly-background.php), and daily global coverage is no longer provided at low latitudes. The second Global Ozone Monitoring Experiment (GOME-2 on MetOp-A/B) also provides daily SO$_2$ measurements but has data gaps between orbits at low latitudes.

Although large, relatively infrequent explosive eruptions releasing ~10 Tg of SO$_2$ or more have the most acute and measurable effects on climate, smaller, more frequent eruptions producing ~0.1 Tg SO$_2$ could have significant
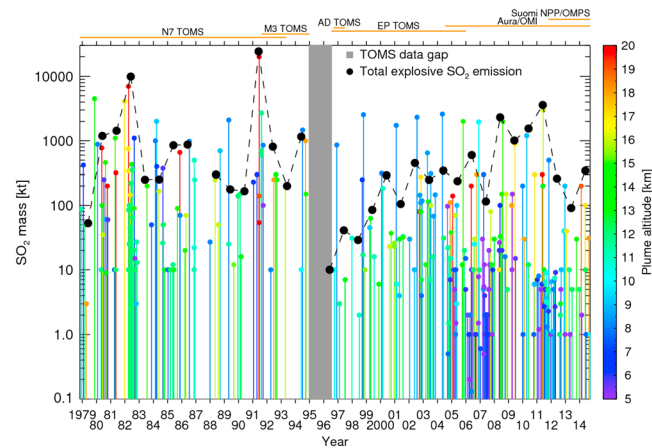
Figure 1. UV satellite measurements of volcanic SO$_2$ emissions by explosive and effusive eruptions from October 1978 to October 2014 based on Total Ozone Mapping Spectrometer (TOMS), Ozone Monitoring Instrument (OMI), and Ozone Mapping and Profiler Suite (OMPS) data. Eruptions are color coded by estimated plume altitude. Plume altitudes are derived from a variety of sources, including Smithsonian Institution Global Volcanism Program volcanic activity reports, volcanic ash advisories, and satellite data (e.g., CALIPSO lidar for eruptions since 2006). The annual total explosive volcanic SO$_2$ production (omitting SO$_2$ discharge from effusive eruptions) is shown in black. The orange lines above the plot indicate the operational lifetimes of the UV satellite instruments: Nimbus-7 (N7); Meteor-3 (M3); ADEOS (AD); and Earth Probe (EP) TOMS, OMI (currently operational), and OMPS (currently operational). The chart only depicts SO$_2$ emissions from discrete volcanic eruptions; continuous emissions from passive degassing and some smaller eruptions are not included. A total of 370 eruptions are shown, releasing a total of ~94 Tg of SO$_2$ (mean = 0.25 Tg). The data shown in this plot will soon be available from the NASA Goddard Earth Sciences (GES) Data and Information Services Center (DISC) as a level 4 Making Earth System Data Records for Use in Research Environments data product.

impacts on decadal time scales [e.g., *Miles et al.*, 2004]. The current inventory of VSO$_2$ emissions (1978–2014), primarily based on Total Ozone Mapping Spectrometer (TOMS) [*Krueger*, 1983; *Krueger et al.*, 1995] and OMI data, is shown in Figure 1. The observed increase in total explosive VSO$_2$ emissions after 2000 occurred concomitantly with a gradual increase in SAOD from post-Pinatubo background levels [e.g., *Solomon et al.*, 2011], which has been attributed to the impact of frequent, small tropical volcanic eruptions [*Vernier et al.*, 2011; *Neely et al.*, 2013]. The UV satellite SO$_2$ data support the conclusions of *Vernier et al.* [2011] and *Neely et al.* [2013] that elevated SAOD has been driven by volcanic eruptions, rather than anthropogenic SO$_2$ emissions [*Hofmann et al.*, 2009], and this increase in SAOD has in turn been implicated in the global warming "hiatus" observed since 1998 [e.g., *Solomon et al.*, 2011; *Santer et al.*, 2014]. Since it appears that the majority of recent SAOD variability (and hence radiative forcing) can be attributed to volcanic eruptions, *Neely et al.* [2013] contend that SAOD should be treated as being continuously and randomly perturbed by volcanic injections, rather

than as a simple trend. Continued space-based monitoring of volcanic SO$_2$ emissions is thus essential, since these measurements of SO$_2$ loading and SO$_2$ altitude [e.g., *Yang et al.*, 2009] can be used to rapidly predict the evolution of SAOD following significant volcanic eruptions.

Hence, we report here the first VSO$_2$ measurements using the OMPS-NM instrument, launched into orbit on 28 October 2011 aboard the SNPP spacecraft, the first of several OMPS missions planned for the next decade and beyond on the Joint Polar Satellite System (JPSS) spacecraft. *Yang et al.* [2013] have previously reported OMPS-NM retrievals of anthropogenic SO$_2$. We focus on the February 2013 eruption of Paluweh volcano (Indonesia) to demonstrate OMPS-NM's sensitivity to small volcanic eruptions in the tropics.

2. The OMPS-NM Instrument and SO$_2$ Retrievals

OMPS-NM is a nadir-viewing hyperspectral instrument that measures backscattered ultraviolet radiance spectra in the 300–380 nm wavelength range at a spectral resolution of 1 nm. SNPP is in a Sun-synchronous, polar orbit, with a local ascending (northbound) equator crossing time at 1:30 P.M. (close to the Aura/OMI overpass at 1:45 P.M. local time). Daily global coverage is achieved using a charge-coupled device detector array that covers a 2800 km cross-track swath (110° FOV) with a nadir pixel size of 50 × 50 km, significantly larger than OMI's 13 × 24 km nadir footprint. However, once per week (currently on Saturdays), OMPS measures in a spatial zoom mode with a nadir pixel size of 10 × 10 km (Figure 2), providing increased sensitivity to small SO$_2$ plumes at the expense of increased noise. Availability of OMPS-NM zoom mode data is currently limited due to bandwidth restrictions on data received from SNPP, but this situation could change on future JPSS/OMPS missions.

Despite its lower spatial resolution than OMI, OMPS-NM offers several improvements over other operational hyperspectral UV imagers, including the use of a single-detector array to cover its entire spectral range,

Figure 2. (left) OMPS-NM zoom-mode lower stratospheric (STL) SO_2 retrieval for the Paluweh volcanic cloud at ~05:10 UTC on 3 February 2013. The gray regions are areas of high reflectivity (>80%) which have been screened to remove retrieval artifacts. (right) The near-coincident AIRS SO_2 retrieval [*Prata and Bernardo*, 2007] at ~05:40 UTC. Both maps show SO_2 vertical column amounts in Dobson units (DU), where $1 \text{ DU} = 2.69 \times 10^{16}$ molecules cm^{-2}. Paluweh volcano is indicated on each map.

yielding a high signal-to-noise ratio at the wavelengths used for SO_2 retrievals. Both OMI and the second Global Ozone Monitoring Experiment (GOME-2 on MetOp-A/B) use three or more channels, with a channel boundary near 310 nm, to cover a broader wavelength range at higher spectral resolution than OMPS-NM [*Levelt et al.*, 2006; *Munro et al.*, 2006], but at the expense of degraded radiances in the 310 nm region, where SO_2 sensitivity is high. Furthermore, OMPS-NM is currently the only operational UV satellite instrument providing daily global coverage at low latitude to midlatitude, due to data gaps in the OMI and GOME-2 measurements.

To retrieve SO_2 vertical column densities (VCDs) from OMPS-NM UV radiances, we have adopted the linear fit (LF) technique currently implemented as the operational OMI SO_2 algorithm for volcanic SO_2 [*Yang et al.*, 2007]. *Yang et al.* [2013] applied a more sophisticated and sensitive spectral fitting algorithm to retrieve anthropogenic SO_2 VCDs using OMPS-NM data, but such sensitivity is not required for VSO_2 in the upper troposphere and lower stratosphere (UTLS). The LF algorithm is computationally fast and efficient and can be used for near real-time SO_2 retrievals for time-critical applications (e.g., aviation hazard mitigation). A key requirement of the LF algorithm is an a priori assumption of the SO_2 vertical profile, for which we use three prescribed profiles representative of VSO_2 in the lower troposphere (TRL product; SO_2 center of mass altitude (CMA) of ~3 km), midtroposphere (TRM product; CMA = ~8 km), and lower stratosphere (STL product; CMA = ~17 km). A detailed LF algorithm description is provided by *Yang et al.* [2007]. For the OMPS-NM SO_2 retrievals, we assume similar error sources to those impacting OMI SO_2 measurements, with an overall uncertainty of ~20% [*Yang et al.*, 2007].

For comparison with the OMPS-NM SO_2 data, we use operational OMI SO_2 retrievals derived using the same LF algorithm (level 2 OMSO2 data product, collection 3) and IR AIRS SO_2 retrievals derived from the level 1B IR geolocated and calibrated radiance product (AIRIBRAD version 5) using the *Prata and Bernardo*'s [2007] algorithm. We have also used the Aura Microwave Limb Sounder (MLS) [*Waters et al.*, 2006] level 2 daily sulfur dioxide product, collection 3 (ML2SO2.003) to verify the altitude of the VSO_2 cloud using MLS-retrieved profiles of UTLS SO_2 mixing ratios. OMSO2, AIRIBRAD, and ML2SO2 data products are all available from the NASA Goddard Earth Sciences (GES) Data and Information Services Center (DISC; http://disc.sci.gsfc.nasa.gov/).

To obtain information on volcanic cloud altitude, we exploit stratospheric aerosol features detected by the Cloud-Aerosol Lidar with Orthogonal Polarization (CALIOP) level 2 lidar vertical feature mask (VFM) product (version 3.02; CAL_LID_L2_VFM-ValStage1-V3-02) [*Vaughan et al.*, 2009] from the CALIPSO satellite [*Winker et al.*, 2009], available from NASA Langley's Atmospheric Science Data Center (http://www-calipso.larc.nasa.gov/). The CALIOP VFM classifies elements in each lidar scene as one of clear air, cloud, aerosol (tropospheric), stratospheric feature (polar stratospheric cloud or stratospheric aerosol), surface, subsurface, or totally attenuated (no signal). In our analysis, we selected all stratospheric features identified by the VFM in nighttime CALIOP overpasses in the vicinity of the Paluweh volcanic cloud between 9 and 12 February 2013.
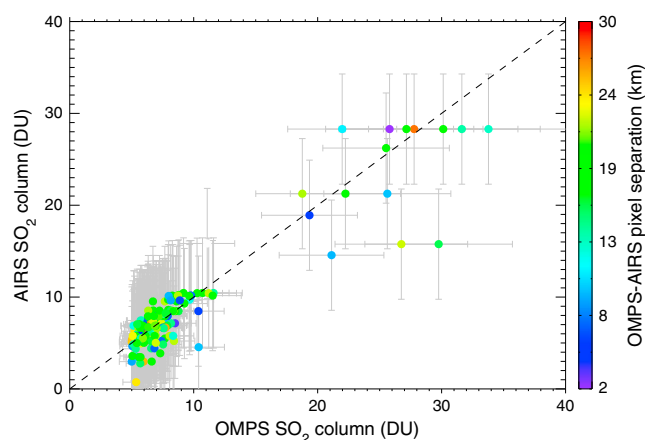
Figure 3. Scatterplot of AIRS SO$_2$ column against OMPS-NM lower stratospheric SO$_2$ column for all OMPS-NM pixels containing ≥5 DU SO$_2$ in the Paluweh volcanic cloud on 3 February 2013. For each OMPS-NM pixel, the AIRS SO$_2$ pixel containing the closest SO$_2$ column amount within a 0.2° (~22 km) search radius around the center of the OMPS-NM pixel is plotted. This attempts to compensate for the expected spatial offsets due to differences in overpass time between OMPS-NM and AIRS (based on wind speeds shown in Figure S1 in the supporting information). The pixels are color coded by OMPS-AIRS pixel separation distance (kilometer). The error bars (gray) are ±6 DU for AIRS [*Prata and Bernardo*, 2007] and ±20% for OMPS-NM, after *Yang et al.* [2007].

3. The 2013 Paluweh Eruption

Paluweh volcano (8.32°S, 121.71°E, elevation 875 m; also known as Rokatenda) forms a small island north of Flores in the Lesser Sunda Islands (East Nusa Tenggara province), Eastern Indonesia. Prior to 2013, the eruptive history of the volcano includes several moderate explosive eruptions (volcanic explosivity index (VEI) of 3), most recently in 1972 [*Siebert et al.*, 2010]. Its largest known historical eruption in 1928 resulted in ashfall in East Java (~850 km west of Paluweh) and a tsunami generated by the collapse of a lava dome into the Flores Sea [*Neumann van Padang*, 1930].

The February 2013 eruption of Paluweh was heralded by explosions at 23:00 local time (15:00 UTC) on 2 February [*Global Volcanism Program*, 2014]. The Darwin Volcanic Ash Advisory Centre (VAAC; ftp://ftp.bom.gov.au/anon/gen/vaac/2013/) issued its first volcanic ash advisory (VAA) for the eruption at 19:26 UTC on 2 February and reported an eruption cloud drifting south at 13.1–13.7 km altitude at 18:32 UTC. The final VAA for the volcanic cloud was issued at 03:32 UTC on 4 February, citing ash at 7–8 km altitude. The Paluweh volcanic cloud resulted in flight delays and other impacts to tourism and aviation as it drifted over the Kimberley coast in Western Australia [*Global Volcanism Program*, 2014]. Based on available reports of only light ashfall on Flores (~60 km S) and no reported tsunami, we infer that the 2013 eruption was of significantly lower magnitude than the 1928 eruption (which has been assigned a VEI of 3).

4. Results

Since the Paluweh eruption began at night, the IR AIRS instrument provided the first SO$_2$ measurements for the eruption, detecting ~0.008 Tg SO$_2$ over the volcano at 17:20 UTC on 2 February and ~0.03 Tg SO$_2$ at 06:20 UTC on 3 February (Figure 2). OMI measurements were affected by the row anomaly on 3 February, but OMPS-NM was in spatial zoom mode (10 × 10 km pixels). Due to their higher spatial resolution (lower signal to noise), OMPS-NM zoom-mode SO$_2$ data are noisier than standard mode measurements, but Figure 2 shows the excellent spatial agreement between near-coincident OMPS-NM and AIRS SO$_2$ retrievals for the Paluweh volcanic cloud on 3 February. However, the SO$_2$ clouds detected by OMPS-NM and AIRS are not precisely collocated due to the ~30 min time difference between the measurements (Figure 2), equivalent to distances of ~15–30 km (or ~1–2 pixels) at the prevailing wind speeds (Figure S1 in the supporting information). A comparison of SO$_2$ column amounts measured by OMPS-NM and AIRS on 3 February is shown in Figure 3. Both OMPS-NM and AIRS measured similar total SO$_2$ loadings in the volcanic cloud (22.2 kt and 26.5 kt, respectively), although Figures 2 and 3 indicate some differences in retrieved SO$_2$ column amounts. The latter are probably due to differences in OMPS-NM and AIRS pixel size, the small but significant difference in overpass time (~30 min) during a period of rapid shearing and dispersion of the volcanic cloud, or the effects of SO$_2$ altitude on the AIRS measurements. Although Figure 3 indicates generally excellent agreement between OMPS-NM and AIRS SO$_2$ retrievals (within measurement uncertainty), there is evidence for a low bias in the AIRS SO$_2$ columns, which has been previously noted in comparisons of UV and IR SO$_2$ retrievals [e.g., *Prata and Bernardo*, 2007]. We attribute this to the higher sensitivity of the UV measurements to tropospheric SO$_2$, resulting in slightly higher UV SO$_2$ columns, where the volcanic cloud extends deeper into
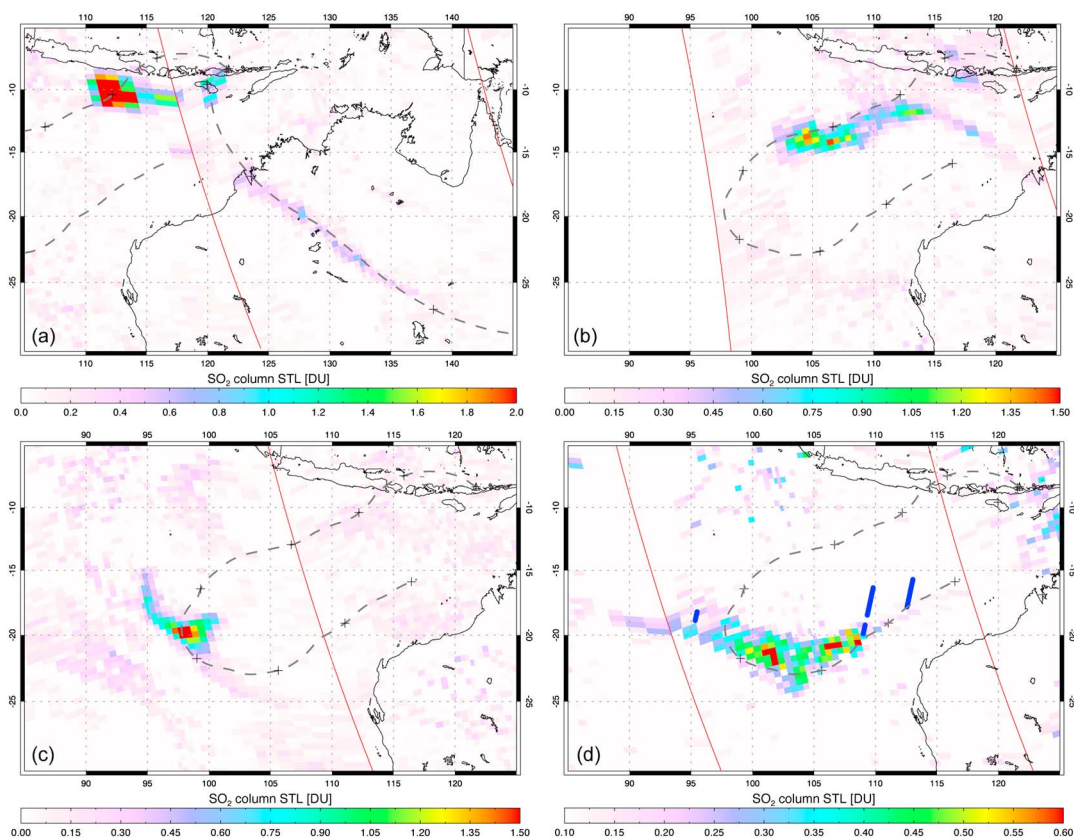
Figure 4. OMPS-NM SO$_2$ retrievals for the February 2013 Paluweh volcanic cloud on (a) 4 February at 04:45–06:30 UTC, (b) 5 February at 06:10–06:15 UTC, (c) 7 February at 07:15 UTC, and (d) 9 February at 06:35–08:20 UTC. The dashed lines show HYSPLIT forward trajectories initialized at altitudes of 15 km (eastern trajectory in Figure 4a) and 17 km (western trajectory in Figure 4a and only trajectory in Figures 4b–4d); crosses are plotted on trajectories every 24 h. Paluweh volcano is indicated by a triangle. The red lines indicate the edges of OMPS-NM orbit swaths. The blue circles in Figure 4d indicate the location of stratospheric aerosol layers identified by the CALIOP vertical feature mask (VFM) algorithm on 9, 10, and 12 February. See also Figure S1 in the supporting information.

the troposphere. This is also evident in Figure 2, where a small tropospheric SO$_2$ plume emerging from Paluweh is detected by OMPS-NM but not by AIRS.

Figure 4 shows the subsequent transport of the Paluweh volcanic SO$_2$ cloud from 4 to 9 February. Note that the SO$_2$ cloud was detected daily from 3 to 10 February, but only a selection of SO$_2$ retrievals is shown here (see Figure S2 in the supporting information). In Figure 4, we also show forward trajectories at altitudes of 15 and 17 km derived from the online Hybrid Single-Particle Lagrangian Integrated Trajectory (HYSPLIT_4) model [*Draxler and Rolph*, 2014; *Rolph*, 2014]. These trajectories closely match the observed SO$_2$ transport and clearly show that while a small amount of SO$_2$ from Paluweh was transported across Australia in the subtropical jet at altitudes of ~15–16 km, most of the SO$_2$ reached the tropopause at ~17 km, following a curved trajectory over the Indian Ocean (Figures 4b–4d). Thus, the SO$_2$ cloud altitude was significantly higher than the volcanic ash plume altitude reported by the Darwin VAAC, likely due to the fact that VAAC observations focus on volcanic ash detection in visible/IR imagery and ash sediments to lower altitudes much more rapidly than volcanic gases such as SO$_2$. The high altitude reached by the Paluweh SO$_2$ cloud is also confirmed by MLS measurements, which detected SO$_2$ at altitudes of ~16–18 km on 4 February 4 (Figure S3 in the supporting information) collocated with the SO$_2$ cloud detected by OMPS-NM south of Java (Figure 4a).

The high altitude reached by aerosol derived from the Paluweh SO$_2$ emissions is corroborated by CALIOP observations from CALIPSO (Figure 4 and Figures S4 and S5 in the supporting information). The CALIOP VFM algorithm identified stratospheric aerosol layers collocated with the dispersing Paluweh SO$_2$ cloud at altitudes of 17–18 km on 9, 10, and 12 February (Figure 4 and Figure S4 in the supporting information), with

CARN ET AL.   929
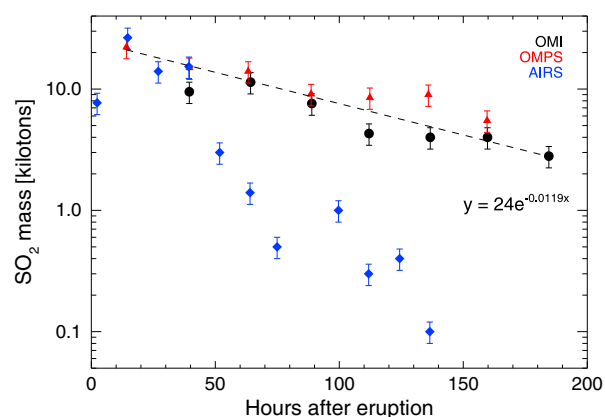
Figure 5. Time series of SO_2 loadings in the Paluweh volcanic cloud from OMI (circles), OMPS (triangles), and AIRS (diamonds) assuming an initial emission at 15:00 UTC on 2 February 2013. An exponential fit to the OMI and OMPS data yields an e-folding time for SO_2 removal of ~84 h (3–4 days). Data are provided in Table S1 in the supporting information.

weakly backscattering aerosol layers with low depolarization (indicating a predominance of liquid phase particles but likely also some aspherical particles producing nonzero depolarization), not detected automatically by the VFM algorithm, also apparent on 7 and 8 February (Figure S5 in the supporting information). CALIOP and AIRS observations (Figures S4, S5, and S6 in the supporting information) also indicate an absence of any significant deep convection that could provide an alternative source for stratospheric particles at this location on 8–12 February (e.g., high-altitude cirrus). These observations, coupled with the increasing CALIOP signal strength with time (e.g., Figures S4 and S5 in the supporting information), indicating sulfate aerosol formation from SO_2, strongly support a volcanic origin for the aerosol. A radiosonde sounding from Learmonth Airport, Western Australia (YPLM; 22.24°S, 114.09°E), to the east of the Paluweh volcanic cloud, on 9 February 2013 at 12 Z (obtained from http://weather.uwyo.edu/upperair/sounding.html; Figure S7 in the supporting information) indicates a cold-point tropopause altitude of ~16.5 km, verifying that the Paluweh aerosols were in the lower stratosphere at this time.

A time series of total SO_2 mass loadings in the Paluweh volcanic cloud from 2 to 10 February, 2013 derived from OMPS-NM, OMI, and AIRS is shown in Figure 5 (see also Table S1 in the supporting information). Figure 5 shows the generally excellent agreement between SO_2 loadings derived from OMI and OMPS-NM, with reported amounts within the 20–30% measurement error [*Yang et al.*, 2007]. Slightly higher SO_2 loadings detected by OMPS-NM on several days are due to the OMI row anomaly reducing the OMI SO_2 loadings when the data gap intersected portions of the drifting volcanic cloud. While AIRS SO_2 loadings are also comparable to OMPS-NM and OMI in the young volcanic cloud, they decay more rapidly than the UV-derived loadings (Figure 5 and Table S1 in the supporting information). We attribute this to a fairly rapid reduction in SO_2 columns below the AIRS detection limit (~6 Dobson unit (DU)) [*Prata and Bernardo*, 2007] as the volcanic cloud dispersed. However, the location of the VSO2 near the cold-point tropopause (Figure S5 in the supporting information) likely increased the AIRS SO_2 sensitivity, allowing the cloud to be detected for several days, due to maximum thermal IR contrast between the absorber (SO_2 plume) at the cold point and the background (warm surface/low clouds).

The decay of SO_2 loading in the volcanic cloud yields an e-folding time for SO_2 removal (which includes conversion to sulfate aerosol and dispersion below satellite detection limits) of ~3–4 days (Figure 5). This is somewhat faster than e-folding times calculated for other recent stratospheric volcanic SO_2 clouds, including ~24 days for Soufrière Hills (Montserrat) in May 2006 [*Prata et al.*, 2007], ~8–9 days for Kasatochi (Alaska) in August 2008 [*Krotkov et al.*, 2010], and ~10–15 days for Grimsvötn (Iceland) in May 2011 [*Sigmarsson et al.*, 2013]. However, this may reflect the location of Paluweh within the Intertropical Convergence Zone (ITCZ), with abundant tropospheric water vapor available for entrainment in the volcanic plume to promote relatively rapid conversion of SO_2 to sulfate. The e-folding time for the Paluweh SO_2 appears to be comparable to that calculated for the November 2010 eruption of Merapi (Java, Indonesia), which also occurred within the ITCZ and resulted in a similar pattern of SO_2 dispersion (S.A. Carn, unpublished data).

5. Discussion

The SO_2 column maps in Figures 2 and 4 and Figure S2 in the supporting information demonstrate the high sensitivity of OMPS-NM to VSO2 in the UTLS, validating its use for extension of the long-term VSO2 emission inventory derived from UV satellite measurements (Figure 1). We have also shown that the February 2013 Paluweh eruption, assigned a low VEI of 2 in the Smithsonian Institution Global Volcanism Program database

(http://www.volcano.si.edu), injected SO_2 to higher altitudes than reported for the ash cloud, and impacted the UTLS. The Paluweh eruption produced ~0.03 Tg SO_2, equivalent to 0.015 Tg S. This sulfur would yield a total sulfate aerosol mass of ~0.04 Tg, assuming that the measured SO_2 is completely oxidized to gaseous H_2SO_4 and then condensed into a 75%–25% H_2SO_4-H_2O solution. Assuming that all the emitted SO_2 reached the stratosphere, this eruption alone would account for the 0.015–0.02 Tg S yr^{-1} needed to sustain the average SAOD trend of 4–7% yr^{-1} after 2002 recognized by *Hofmann et al.* [2009] and subsequently confirmed by other studies [*Nagai et al.*, 2010; *Vernier et al.*, 2011]. Although an order of magnitude smaller than other recent tropical eruptions such as Soufrière Hills in May 2006 [*Prata et al.*, 2007] and Tavurvur (Rabaul, Papua New Guinea) in October 2006, which significantly perturbed tropical SAOD in 2006–2007 [*Vernier et al.*, 2011], eruptions similar to Paluweh may maintain SAODs at levels above the true "nonvolcanic" background and contribute to observed SAOD trends. We note that Soputan volcano (northern Sulawesi, Indonesia) also frequently injects SO_2 into the tropical UTLS [*Kushendratno et al.*, 2012].

Events such as the Paluweh eruption are important to recognize as studies focused on the climatic impacts of volcanic eruptions typically use a threshold of VEI$\geq$3 or 4 to filter those capable of impacting SAOD [e.g., *Deshler et al.*, 2006; *Vernier et al.*, 2011; *Neely et al.*, 2013] and thus may omit important perturbations or implicate nonvolcanic sources [e.g., *Hofmann et al.*, 2009]. We therefore recommend that analyses of the impacts of small volcanic eruptions on climate [e.g., *Vernier et al.*, 2011] avoid the use of VEI to establish the sources of SAOD perturbations but instead use direct satellite measurements of SO_2 loading and altitude (e.g., Figure 1), which can now be produced rapidly from a number of operational satellite instruments. Furthermore, the use of VEI to assign volcanic plume (SO_2) altitude in climate models is also flawed, since SO_2 emitted by tropical eruptions is capable of reaching the tropopause due to moist convection [e.g., *Tupper et al.*, 2009], regardless of eruption magnitude. Similarly, the Paluweh case demonstrates that reported plume altitudes may be biased low and hence cannot always be used to infer eruption magnitude and SO_2 release [e.g., *Diehl et al.*, 2012], and hence stratospheric impact. *Tupper and Wunderman* [2009] report a low bias in volcanic plume heights reported from the ground, and this may be a pervasive problem for tropical eruptions. Small VSO$_2$ injections into the UTLS are therefore more common than apparent from current volcanic activity databases.

6. Conclusions

This analysis of the 2013 Paluweh eruption confirms the sensitivity of the OMPS-NM sensor aboard Suomi-NPP to VSO$_2$ in the UTLS, and the ability of OMPS-NM data to continue the long-term record of VSO$_2$ emissions begun by TOMS in 1978. The altitude reached by the Paluweh volcanic SO_2 cloud was determined based on matching HYSPLIT trajectories with the observed SO_2 cloud trajectory from OMPS observations and was found to be significantly higher (~17 km) than the reported ash column altitude (~13–14 km). Such eruption clouds lofted to the tropopause are easy to detect with IR satellite sensors, which achieve maximum sensitivity to SO_2 at the cold point. Stratospheric aerosol presence following the eruption was confirmed using CALIPSO lidar observations. The Paluweh eruption demonstrates that even relatively small explosive eruptions with unremarkable VEIs (VEI < 3) may inject SO_2 to tropopause altitudes or higher, emphasizing the potential impact of small tropical volcanic eruptions on SAOD. This low bias in SO_2 cloud altitudes may be pervasive in eruption reports and may result in an underestimate of volcanic impacts on SAOD. Using VEI alone to estimate SO_2 injection altitude is inadvisable for tropical eruptions.

References

Bluth, G. J. S., C. C. Schnetzler, A. J. Krueger, and L. S. Walter (1993), The contribution of explosive volcanism to global atmospheric sulfur dioxide concentrations, *Nature*, *366*, 327–329.

Carn, S. A., A. J. Krueger, G. J. S. Bluth, S. J. Schaefer, N. A. Krotkov, I. M. Watson, and S. Datta (2003), Volcanic eruption detection by the Total Ozone Mapping Spectrometer (TOMS) instruments: A 22 year record of sulfur dioxide and ash emissions, in *Volcanic Degassing*, edited by C. Oppenheimer, D. M. Pyle, and J. Barclay, *Geol. Soc. London Spec. Publ.*, *213*, 177–202.

Clarisse, L., D. Hurtmans, C. Clerbaux, J. Hadji-Lazaro, Y. Ngadi, and P.-F. Coheur (2012), Retrieval of sulphur dioxide from the infrared atmospheric sounding interferometer (IASI), *Atmos. Meas. Tech.*, *5*, 581–594, doi:10.5194/amt-5-581-2012.

Deshler, T., R. Anderson-Sprecher, H. Jäger, J. Barnes, D. J. Hofmann, B. Clemesha, D. Simonich, M. Osborn, R. G. Grainger, and S. Godin-Beekmann (2006), Trends in the nonvolcanic component of stratospheric aerosol over the period 1971–2004, *J. Geophys. Res.*, *111*, D01201, doi:10.1029/2005JD006089.

Diehl, T., A. Heil, M. Chin, X. Pan, D. Streets, M. Schultz, and S. Kinne (2012), Anthropogenic, biomass burning, and volcanic emissions of black carbon, organic carbon, and SO_2 from 1980 to 2010 for hindcast model experiments, *Atmos. Chem. Phys. Discuss.*, *12*, 24,895–24,954, doi:10.5194/acpd-12-24895-2012.

Draxler, R. R., and G. D. Rolph (2014), HYSPLIT (HYbrid Single-Particle Lagrangian Integrated Trajectory) Model access via NOAA ARL READY Web site, Available at http://ready.arl.noaa.gov/HYSPLIT.php, NOAA Air Resources Laboratory, Silver Spring, Md.

Global Volcanism Program (2014), Report on Paluweh (Indonesia), in *Bulletin of the Global Volcanism Network*, vol. 39, edited by R. Wunderman, Smithsonian Inst., doi:10.5479/si.GVP.BGVN201401-264150.

Hofmann, D., J. Barnes, M. O'Neill, M. Trudeau, and R. Neely (2009), Increase in background stratospheric aerosol observed with lidar at Mauna Loa Observatory and Boulder, Colorado, *Geophys. Res. Lett.*, *36*, L15808, doi:10.1029/2009GL039008.

Krotkov, N. A., M. R. Schoeberl, G. A. Morris, S. Carn, and K. Yang (2010), Dispersion and lifetime of the SO_2 cloud from the August 2008 Kasatochi eruption, *J. Geophys. Res.*, *115*, D00L20, doi:10.1029/2010JD013984.

Krueger, A. J. (1983), Sighting of El Chichón sulfur dioxide clouds with the Nimbus 7 Total Ozone Mapping Spectrometer, *Science*, *220*, 1377–1378.

Krueger, A. J., L. S. Walter, P. K. Bhartia, C. C. Schnetzler, N. A. Krotkov, I. Sprod, and G. J. S. Bluth (1995), Volcanic sulfur dioxide measurements from the Total Ozone Mapping Spectrometer (TOMS) instruments, *J. Geophys. Res.*, *100*(D7), 14,057–14,076, doi:10.1029/95JD01222.

Kushendratno, J. S. Pallister, Kristianto, F. R. Bina, W. McCausland, S. A. Carn, N. Haerani, J. Griswold, and R. Keeler (2012), Recent explosive eruptions and volcano hazards at Soputan volcano: A basalt stratovolcano in north Sulawesi, Indonesia, *Bull. Volcanol.*, *74*(7), 1581–1609.

Levelt, P. F., G. H. J. van den Oord, M. R. Dobber, A. Mälkki, H. Visser, J. de Vries, P. Stammes, J. O. V. Lundell, and H. Saari (2006), The Ozone Monitoring Instrument, *IEEE Trans. Geosci. Remote Sens.*, *44*(5), 1093–1101, doi:10.1109/TGRS.2006.872333.

Miles, G. M., R. G. Grainger, and E. J. Highwood (2004), The significance of volcanic eruption strength and frequency for climate, *Q. J. R. Meteorol. Soc.*, *130*, 2361–2376.

Munro, R., M. Eisinger, C. Anderson, J. Callies, E. Corpaccioli, R. Lang, A. Lefebvre, Y. Livschitz, and A. Perez Albinana (2006), GOME-2 on MetOp, paper presented at the *2006 EUMETSAT Meteorological Satellite Conference*, Eur. Org. for the Exploit of Meteorol. Satell., Helsinki.

Nagai, T., B. Liley, T. Sakai, T. Shibata, and O. Uchino (2010), Post-Pinatubo evolution and subsequent trend of the stratospheric aerosol layer observed by mid-latitude lidars in both hemispheres, *SOLA*, *6*, 69–72, doi:10.2151/sola.2010-018.

Neely, R. R., III et al. (2013), Recent anthropogenic increases in SO_2 from Asia have minimal impact on stratospheric aerosol, *Geophys. Res. Lett.*, *40*, 999–1004, doi:10.1002/grl.50263.

Neumann van Padang, M. (1930), Paloeweh, *Vulk. Seism. Meded. Dienst. Mijnw. Ned-Indie*, *11*, 1–141.

Prata, A. J., and C. Bernardo (2007), Retrieval of volcanic SO_2 column abundance from Atmospheric Infrared Sounder data, *J. Geophys. Res.*, *112*, D20204, doi:10.1029/2006JD007955.

Prata, A. J., S. A. Carn, A. Stohl, and J. Kerkmann (2007), Long range transport and fate of a stratospheric volcanic cloud from Soufrière Hills volcano, Montserrat, *Atmos. Chem. Phys.*, *7*, 5093–5103.

Robock, A. (2000), Volcanic eruptions and climate, *Rev. Geophys.*, *38*, 191–219, doi:10.1029/1998RG000054.

Rolph, G. D. (2014), Real-time Environmental Applications and Display sYstem (READY) Web site, Available at http://ready.arl.noaa.gov, NOAA Air Resources Laboratory, Silver Spring, Md.

Santer, B. D., et al. (2014), Volcanic contribution to decadal changes in tropospheric temperature, *Nat. Geosci.*, *7*, 185–189, doi:10.1038/ngeo2098.

Siebert, L., T. Simkin, and P. Kimberly (2010), *Volcanoes of the World*, 3rd ed., Univ. of Calif. Press, Berkeley and Los Angeles.

Sigmarsson, O., B. Haddadi, S. Carn, S. Moune, J. Gudnason, K. Yang, and L. Clarisse (2013), The sulfur budget of the 2011 Grímsvötn eruption, Iceland, *Geophys. Res. Lett.*, *40*, 1–6, doi:10.1002/2013GL057760.

Solomon, S., J. S. Daniel, R. R. Neely III, J.-P. Vernier, E. G. Dutton, and L. W. Thomason (2011), The persistently variable "background" stratospheric aerosol layer and global climate change, *Science*, *333*, 866–870.

Tupper, A., and R. Wunderman (2009), Reducing discrepancies in ground and satellite-observed eruption heights, *J. Volcanol. Geotherm. Res.*, *186*, 22–31.

Tupper, A., C. Textor, M. Herzog, H.-F. Graf, and M. S. Richards (2009), Tall clouds from small eruptions: The sensitivity of eruption height and fine ash content to tropospheric instability, *Nat. Hazards*, *51*, 375–401.

Vaughan, M. A., K. A. Powell, D. M. Winker, C. A. Hostetler, R. E. Kuehn, W. H. Hunt, B. J. Getzewich, S. A. Young, Z. Liu, and M. J. McGill (2009), Fully automated detection of cloud and aerosol layers in the CALIPSO lidar measurements, *J. Atmos. Oceanic Tech.*, *26*, 2034–2050.

Vernier, J. P., et al. (2011), Major influence of tropical volcanic eruptions on the stratospheric aerosol layer during the last decade, *Geophys. Res. Lett.*, *38*, L12807, doi:10.1029/2011GL047563.

Waters, J. W., et al. (2006), The Earth Observing System Microwave Limb Sounder (EOS MLS) on the Aura satellite, *IEEE T. Geosci. Remote Sens.*, *44*(5), 1075–1092.

Winker, D. M., M. A. Vaughan, A. Omar, Y. Hu, K. A. Powell, Z. Liu, W. H. Hunt, and S. A. Young (2009), Overview of the CALIPSO mission and CALIOP aata processing algorithms, *J. Atmos. Oceanic Tech.*, *26*, 2310–2323.

Yang, K., N. A. Krotkov, A. J. Krueger, S. A. Carn, P. K. Bhartia, and P. F. Levelt (2007), Retrieval of large volcanic SO_2 columns from the Aura Ozone Monitoring Instrument: Comparison and limitations, *J. Geophys. Res.*, *112*, D24S43, doi:10.1029/2007JD008825.

Yang, K., X. Liu, N. A. Krotkov, A. J. Krueger and S. A. Carn (2009), Estimating the altitude of volcanic sulfur dioxide plumes from space-borne hyperspectral UV measurements, *Geophys. Res. Lett.*, *36*, L10803, doi:10.1029/2009GL038025.

Yang, K., R. R. Dickerson, S. A. Carn, C. Ge, and J. Wang (2013), First observations of SO_2 from the satellite Suomi NPP OMPS: Widespread air pollution events over China, *Geophys. Res. Lett.*, *40*, doi:10.1002/grl.50952.